

NANO EXPRESS

Open Access



Enhanced Crystallinity of Triple-Cation Perovskite Film via Doping NH_4SCN

Ziji Liu^{1*†}, Detao Liu^{1†}, Hao Chen¹, Long Ji¹, Hualin Zheng¹, Yiding Gu¹, Feng Wang¹, Zhi Chen^{1,2*} and Shibin Li^{1*}

Abstract

The trap-state density in perovskite films largely determines the photovoltaic performance of perovskite solar cells (PSCs). Increasing the crystal grain size in perovskite films is an effective method to reduce the trap-state density. Here, we have added NH_4SCN into perovskite precursor solution to obtain perovskite films with an increased crystal grain size. The perovskite with increased crystal grain size shows a much lower trap-state density compared with reference perovskite films, resulting in an improved photovoltaic performance in PSCs. The champion photovoltaic device has achieved a power conversion efficiency of 19.36%. The proposed method may also impact other optoelectronic devices based on perovskite films.

Keywords: Perovskite solar cells, NH_4SCN , Crystalline, Trap-state density

Introduction

Owing to the excellent optoelectronic properties, the organic-inorganic hybrid metal halide perovskite (OIMHP) has been widely used as the light-harvester material of solar cells. The last certified power conversion efficiency (PCE) of the solar cells based on OIMHP has reached 24.2% [1]. Perovskite solar cells (PSCs) are the most promising solar cells among the third-generation solar cells.

The bandgap of conventional OIMHP films is at the range of 1.5–1.6 eV, and the corresponding theoretical Shockley–Queisser limit efficiency (TS-QLE) is higher than 30% [2–4]. However, the reported highest PCE is much lower than the TS-QLE due to the trap-assisted non-radiative recombination in the perovskite film [5–8]. The trap-assisted non-radiative recombination intensity often depends on the defect density in perovskite films and most of the defects are spread on the surface and boundary of perovskite crystal grains due to the atomic vacancies [7, 9]. Therefore, perovskite films with less crystal grain boundary area contribute to the better photovoltaic performance of

PSCs [10–12]. The perovskite films with less crystal grain boundary area can be obtained via increasing the crystal grain size. To enlarge the crystal grain size of perovskite films, various methods have been developed, including the additive engineering [13–15], precursor solvent engineering [16], anti-solvent engineering [17], and procedure optimization [18–20]. Among these methods, the additive engineering is one of the most frequently used methods to the realization of large-crystal-grain-size perovskite films. The additive materials include polymers [21], small organic molecules [15, 22], and inorganic salts [23]. The polymers with special organic groups like carbonyl groups can slow down the crystallization process and enlarge the grain size of the perovskite films [21]. The carbonyl bonds containing lone electron pairs can interact with the Lewis acid PbI_2 in the precursor solution and the intermediate polymer- PbI_2 adduct forms. The formation of the adduct retards the crystal growth and improves the crystallinity of the perovskite film. Bi et al. employed poly(methyl methacrylate) (PMMA) as a template to control the crystallization process of perovskite, improving the PCE up to 21.6% [21]. Small organic molecules containing special groups are also used frequently to adjust the crystallinity of perovskite films. The mechanism for improving the crystallinity of perovskite is the same as polymers. To avoid the defect formation, the small organic molecules are required to have suitable energy levels. Zhang et al. used a fused ring electron acceptor material to dope

* Correspondence: zjliu@uestc.edu.cn; zhichen@engr.uky.edu; shibinli@uestc.edu.cn

Ziji Liu and Detao Liu contribute equally to this work

†Ziji Liu and Detao Liu contributed equally to this work.

¹State Key Laboratory of Electronic Thin Films and Integrated Devices, and School of Optoelectronic Science and Engineering, University of Electronic Science and Technology of China (UESTC), Chengdu 610054, Sichuan, China
Full list of author information is available at the end of the article

perovskite films. This material improved the crystallinity of perovskite films and increased the PCE of PSCs from 19.6% to 21.7% [22]. The inorganic salts used in perovskite films include $\text{Pb}(\text{SCN})_2$, KSCN , NaSCN , CdCl_2 , and NiCl_2 [14, 24, 25]. The SCN^- has a larger electronegativity than the I^- ionic, so SCN^- anion is more apt to form ionic bonding with the CH_3NH_3^+ cation than the I^- anion. The formed ionic bonding can also retard the crystal growth and increase the crystallinity of perovskite films. When the perovskite was heated at high temperature, the SCN^- can escape from perovskite films and the metal ions can be left. The Cd^{2+} and Ni^{2+} in perovskite precursors can change the crystal growth mechanism and improve the crystallinity of perovskite films.

The ammonium thiocyanate (NH_4SCN) contains SCN^- anion, so it can improve the crystallinity of perovskite films [11]. This material in perovskite films can be decomposed into HSCN and NH_3 when samples are heated on hotpot. Therefore, no residual of NH_4SCN will be left in perovskite films and defects induced by the introduction of NH_4SCN will not appear. From the above analysis, NH_4SCN is an effective additive for improving the crystallinity of perovskite films, which has been proved by Zhang et al. [26]. Chen's group has used NH_4SCN to enhance the crystallinity of FAPbI_3 films and form the vertically oriented 2D-layered perovskite films [27–29]. Ning's group introduced NH_4SCN into tin-based perovskite films to manipulate the crystal growth process, which improved the photovoltaic performance and stability of tin-based PSCs [30].

Here, the NH_4SCN was employed to control the crystallinity of triple-cation perovskite films. The NH_4SCN can increase the crystal grain size and reduce the boundary area in perovskite films, inducing a lower trap-state density. The lower trap-state density attributes to the longer charge lifetime and higher photovoltaic performance of PSCs. The PCE of PSCs has been improved from 17.24% to 19.36%.

Method

Materials

All of the materials were purchased from Ying Kou You Xuan Trade Co., Ltd., if not specified. The PbI_2 , tris(2-(1H-pyrazol-1-yl)-4-tert-butylpyridine)-cobalt(III) bis(trifluoromethylsulphonyl)imide (FK209), PEDOT: PSS, and FAI were purchased from Xi'an Polymer Light Technology Corp. CsI, dimethylformamide (DMF), and dimethyl sulfoxide (DMSO) were purchased from Sigma-Aldrich Corp. The SnO_2 nanoparticle colloidal solution was purchased from Alfa Aesar.

The perovskite solution was prepared as follows: 507 mg PbI_2 , 73.4 mg PbBr_2 , 172 mg FAI and 22.4 mg MABr was dissolved into 1 mL solvent mixture ($\text{V}(\text{DMSO})/\text{V}(\text{DMF}) = 3:7$) to prepare the solution 1. Then, 52- μL

CsI solution (390 mg in 1 mL DMSO) was added into the solution 1 and then the final solution was stirred for 2 h. For the NH_4SCN -doped perovskite solutions, different mass of NH_4SCN was added into the prepared perovskite solutions directly and the final solutions were stirred for 2 h. The HTL solution was prepared by dissolving 72.3 mg (2,29,7,79-tetrakis(*N,N*-di-*p*-methoxyphenylamine)-9,9-spirobifluorene) (spiro-MeOTAD), 28.8 μL 4-tert-butylpyridine, 17.5 μL of a stock solution of 520 mg/mL lithium bis(trifluoromethylsulphonyl)imide in acetonitrile, and 29 μL of a solution of 300 mg/mL FK209 in acetonitrile in 1 mL chlorobenzene.

Preparation

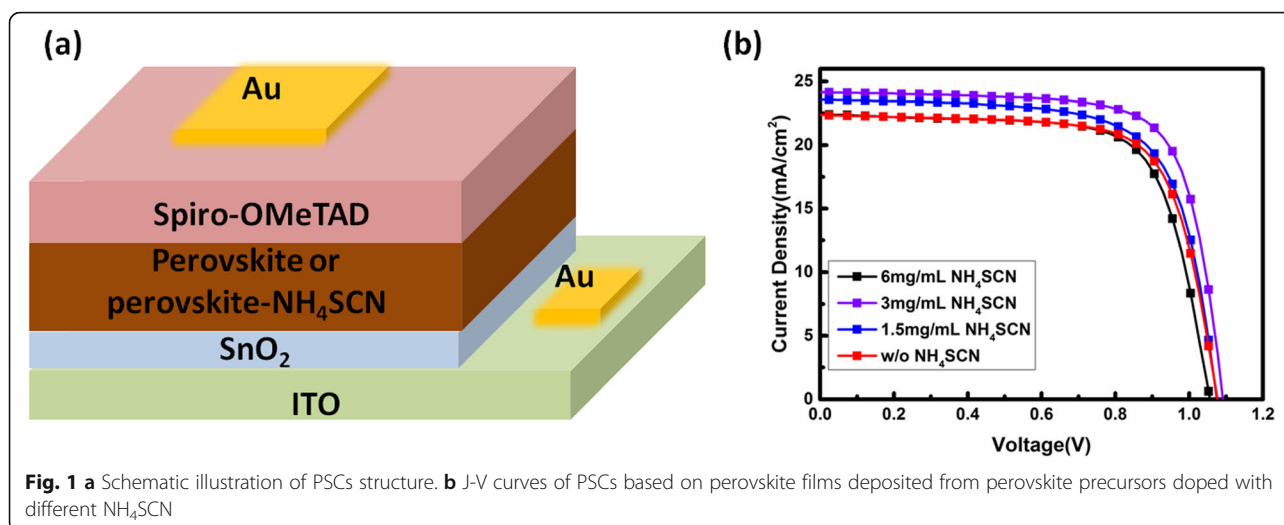
The indium tin oxide (ITO) glasses were cleaned sequentially in acetone, absolute ethyl alcohol, and deionized water ultrasonic bath for 15 min, respectively. After ITO glasses were cleaned by the UV-ozone treat for 20 min, a SnO_2 film was deposited by spin-coating diluted SnO_2 nanoparticle colloidal solution (Alfa Aesar (tin(IV) oxide, 15% in H_2O colloidal dispersion)) according to reference [31]. After the spin-coating, the SnO_2 film was heated at 165 °C for 0.5 h. Then the substrates were treated with the UV-ozone again and transferred into the glovebox. Perovskite films were prepared by spin-coating with a speed of 1000 rpm for 10 s and 5000 rpm for 45 s. At 9 s before the ending of the spin-coating program, 150 μL chlorobenzene was dropped onto the spinning substrate. Then, the perovskite films were heated at 100 °C for 60 min. The HTL was prepared by spin-coating the HTL solution at 5000 rpm for 30 s. Finally, 100 nm of Au top electrode was thermally evaporated onto the HTL.

Characterization

The current density-voltage (J-V) characteristic of PSCs was recorded by Keithley source unit 2400 under AM 1.54G sun intensity illumination by a solar simulator from Newport Corp. The X-ray diffraction patterns were recorded with Bruker D8 ADVANCE A25X. Fourier-transform infrared spectroscopy (FTIR) and scanning electron microscope (SEM) were conducted on Nicolet iS10 and field emission fitting SEM (FEI-Inspect F50, Holland). The absorption of perovskite was measured using Shimadzu 1500 spectrophotometer.

Results and Discussion

To optimize the content of NH_4SCN , perovskite films were deposited using the perovskite precursor solutions doped with different content of NH_4SCN , and these films were used as the light harvester layers of solar cells. The configuration of PSCs is ITO/ SnO_2 /perovskite/Spiro-OMeTAD/Au, as shown in Fig. 1a. To simplify the expression in this article, the perovskite film fabricated



from perovskite precursor solutions doped with a concentration of x mg/mL is expressed as perovskite- x here. The current density-voltage (J-V) curve of the champion device in each group is plotted in Fig. 1b, and the corresponding photovoltaic parameters are listed in Table 1. The statistical data for photovoltaic parameters of PSCs are shown in Fig. 2a–d. The perovskite-1.5-based PSCs (target PSCs) exhibit the best photovoltaic performance, attributed to the improved short-circuit current density (J_{SC}) and fill factor (FF). Compared with the champion perovskite-0-based PSCs (reference PSCs), all the photovoltaic parameters of the champion PSCs based on perovskite-3 have been enhanced obviously, resulting in a PCE of 19.36%. The external quantum efficiency (EQE) spectrums of target PSCs and reference PSCs are shown in Fig. 3a. The EQE values of target PSCs at most of the visible light region are higher than that of reference PSCs, consisting with the EQE result in reference [26]. This phenomenon results from the more efficient charge transport in perovskite films with better crystallinity. To investigate the mechanism for the photovoltaic performance improvement, several characterizations have been carried out on the perovskite films.

The reflecting FTIR measurement has been carried on perovskite films without NH_4SCN doping (perovskite-w/o- NH_4SCN) and perovskite films with NH_4SCN doping (perovskite- NH_4SCN) to identify the organic groups and

ingredients in perovskite films, as shown in Fig. 3a. The absorption peaks at the wavenumber of 1350 cm^{-1} and 1477 cm^{-1} are attributed to the vibration of organic $-\text{CH}_3$ groups in perovskite films. The corresponding absorption peaks of the amino groups in perovskite films locate at the range of $1600\text{--}1750\text{ cm}^{-1}$ and $3200\text{--}3500\text{ cm}^{-1}$. No absorption peak corresponding to $-\text{C}\equiv\text{N}$ in $-\text{SCN}$ can be found in perovskite- NH_4SCN , demonstrating that there is no residue of NH_4SCN in the final perovskite- NH_4SCN films. The UV-visible light absorption also has been measured and the result is shown in Fig. 3b. Both perovskite films have a strong absorption when the light wavelength is below 750 nm , and the absorption edges of both perovskite films overlap, clarifying the bandgap values of both perovskite films are the same. The similar shape of the FTIR plots and UV-visible absorption curves of the perovskite-w/o- NH_4SCN and perovskite- NH_4SCN indicates that both perovskite films have the same ingredient.

The morphology of perovskite films is investigated using SEM, and the results are shown in Fig. 4a, b. The perovskite films without NH_4SCN dopants contain many small-size crystals with a grain size lower than 200 nm . In contrast, there are much fewer small-size crystals in perovskite- NH_4SCN films. The average crystal grain sizes of both perovskite films have been calculated using the Nano Measurer software. The average crystal grain size of perovskite-w/o- NH_4SCN and perovskite- NH_4SCN is about 312.02 nm and 382.95 nm , respectively. The grain-size distributions of the crystals in SEM images are shown in Fig. 4c. The frequency of the crystal grain size distributed at the range of $200\text{--}300\text{ nm}$ is highest in perovskite-w/o- NH_4SCN . However, the frequency of the crystal grain size distributed at the range of $300\text{--}400\text{ nm}$ is highest in perovskite- NH_4SCN . The distribution proportion of the grain size larger than 400 nm in perovskite-w/o- NH_4SCN

Table 1 Photovoltaic parameters of the champion device in each group

Device	J_{SC} (mA/cm^2)	V_{OC} (V)	FF (%)	PCE (%)
Perovskite-0-based PSCs	22.37	1.077	71.58	17.24
Perovskite-1.5-based PSCs	23.57	1.075	69.88	17.71
Perovskite-3-based PSCs	24.17	1.091	73.39	19.36
Perovskite-6-based PSCs	22.45	1.056	71.04	16.85

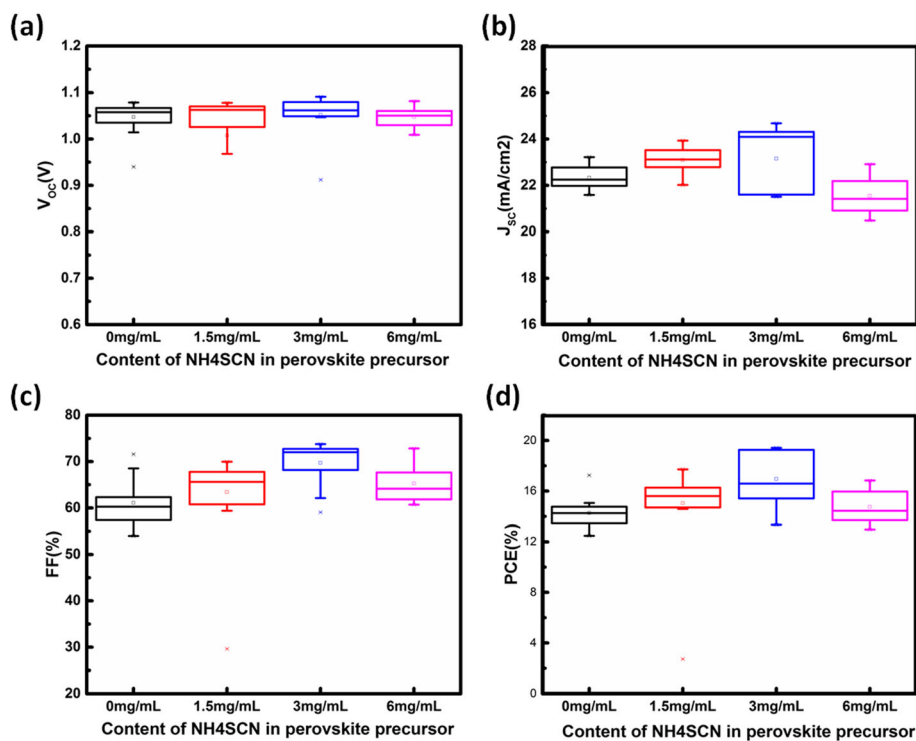


Fig. 2 a–d Statistical data for V_{OC} (a), J_{SC} (b), FF (c), and PCE (d) of PSCs based on perovskite films deposited from perovskite precursors doped with different NH_4SCN

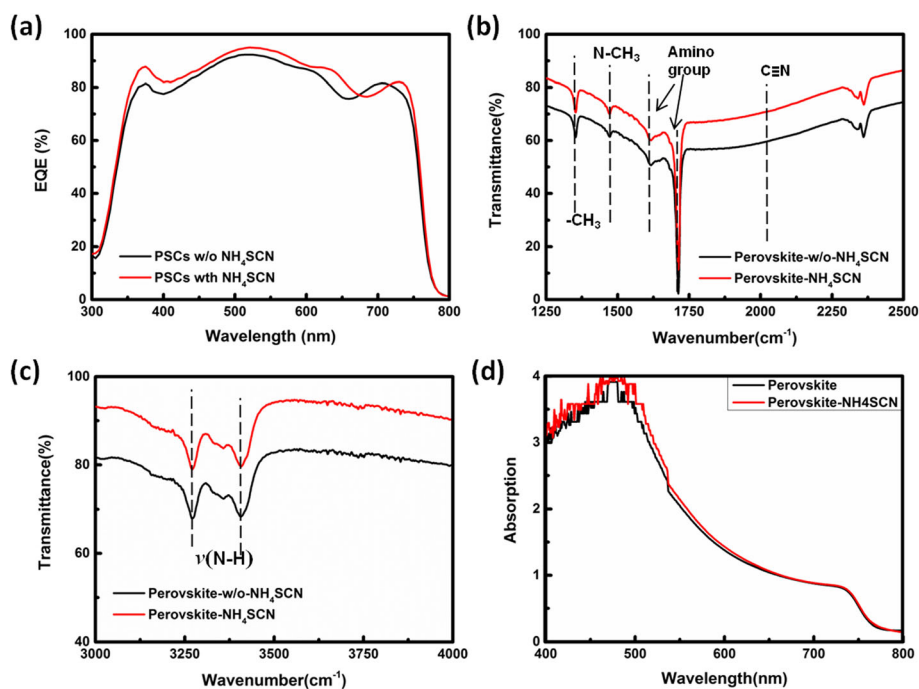


Fig. 3 a EQE spectrum of target PSCs (PSCs with NH_4SCN) and reference PSCs (PSCs w/o NH_4SCN). **b, c** FTIR results of the perovskite-w/o- NH_4SCN films and perovskite- NH_4SCN films. **d** UV-vis absorption spectrum of the perovskite-w/o- NH_4SCN films and perovskite- NH_4SCN films

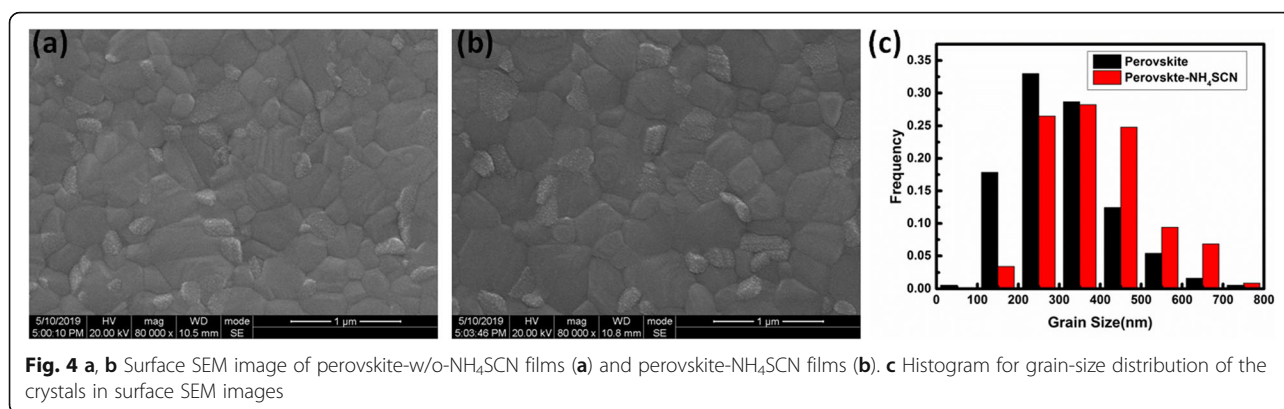


Fig. 4 a, b Surface SEM image of perovskite-w/o-NH₄SCN films (a) and perovskite-NH₄SCN films (b). c Histogram for grain-size distribution of the crystals in surface SEM images

is also much lower than that in perovskite-NH₄SCN. The larger grain size in perovskite results in the fewer crystal grain boundaries. It has been reported that the trap states are mainly distributed on the boundaries of perovskite crystal grains. Hence, the perovskite-NH₄SCN films with larger-size crystal grains are favored by high-performance PSCs.

The X-ray diffraction (XRD) pattern has been used to identify the crystallinity of perovskite films further. There are no distinct peak location shifts in the XRD pattern of perovskite-NH₄SCN films compared with the XRD pattern of perovskite-w/o-NH₄SCN films, demonstrating that both perovskite films show the same crystallization type. The peaks at 14.37°, 20.27°, 24.82°, 28.66°, 32.12°, 35.38°, 40.88°, and 43.46° correspond to (001), (011), (111), (002), (012), (112), (022) and (003) planes of perovskite films, respectively. The peaks at 12.93° originate from the PbI₂ crystal grains. The strongest peak in XRD patterns locates at 14.37°, so we have magnified the XRD patterns at a range of 12–15° to observe the crystallinity difference between these two perovskite films accurately. The PbI₂ peak intensity in the XRD pattern of the perovskite-NH₄SCN is lower than that of the perovskite-w/o-NH₄SCN, indicating that less PbI₂ byproduct can be observed. Except the excess PbI₂ in perovskite precursor, PbI₂ can also be generated when the perovskite is annealed due to the escape of some organic cation salts. Hence, it can be inferred that perovskite-NH₄SCN films show better thermal stability. The (001) plane peak intensity in the XRD pattern of perovskite-NH₄SCN films is higher than that of perovskite-w/o-NH₄SCN, and the (001) plane peak width at half the height in the XRD pattern of perovskite-NH₄SCN films is much smaller, clarifying perovskite-NH₄SCN films show better crystallinity.

The electron-only devices and hole-only devices have been fabricated to characterize the electron trap-state density and hole trap-state density in both perovskite films, respectively. The configuration of electron-only

devices and hole-only devices is presented in the inset of Fig. 5 c and d, respectively. The dark current-voltage (I-V) curves of the devices have been measured and plotted in Fig. 5c, d. All I-V curves contain ohmic response region at low bias voltage region. As the voltage is continuously increased, the current rises steeply due to the reduced trap density. The kink point (V_{TFL}) of these curves can be used to identify the trap-state density according to equation (1) [32–35]:

$$V_{\text{TFL}} = \frac{en_t L^2}{2\epsilon\epsilon_0} \quad (1)$$

where L is the thickness of the perovskite films, ϵ is the relative dielectric constant of perovskite films, n_t is the trap-state density, and ϵ_0 is the vacuum permittivity. The similar absorption intensity shown in Fig. 3b indicated that the thickness of both perovskite films is very close. The FTIR results and UV-visible light absorption edges show that the ingredients in perovskite films are the same. Therefore, both perovskite films have the same ϵ value. The V_{TFL} is relative to the trap-state density positively. As shown in Fig. 5c, d, both V_{TFL} values obtained from perovskite-NH₄SCN-based electron-only devices and perovskite-NH₄SCN-based hole-only devices are obviously lower than those obtained from perovskite-w/o-NH₄SCN-based electron-only devices and perovskite-w/o-NH₄SCN-based hole-only devices. It clarifies that both electron trap-state density and hole trap-state density have been reduced in perovskite-NH₄SCN films due to the increased crystal grain size.

From the above characterization and analysis, we can infer that using perovskite precursor solution doped with NH₄SCN to deposit perovskite films increases the perovskite crystal grain size, resulting in a reduced crystal boundary area and trap-state density. The reduced trap-state density in perovskite is beneficial to the enhanced charge transport and photovoltaic performance of PSCs.

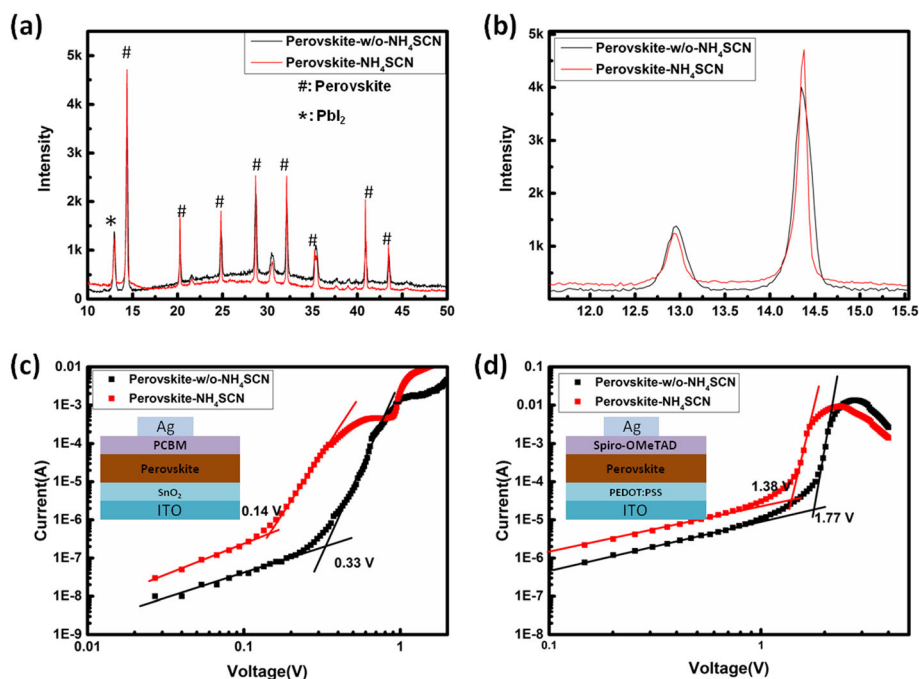


Fig. 5 **a** XRD patterns of perovskite-w/o-NH₄SCN films and perovskite-NH₄SCN films. **b** Magnified XRD patterns at a range of 12–15°. **c** dark I-V curves for electron-only devices based on different perovskite films (inset: configuration of electron-only devices). **d** Dark I-V curves for hole-only devices based on different perovskite films (inset: configuration of hole-only devices)

Conclusion

In conclusion, we have adapted NH₄SCN as the dopant of perovskite precursors to increase the crystalline of perovskite films. The enhanced-crystallinity perovskite-based PSCs achieve the champion PCE of 19.36% which is much higher than the maximum PCE of the reference PSCs (17.24%). The improved photovoltaic performance of target PSCs is attributed to the enhanced crystal grain size in perovskite-NH₄SCN films. The enhanced crystal grain size in perovskite-NH₄SCN films can reduce the charge trap-state density and benefit to the charge transport. Our results demonstrate a simple and effective way to enhance the device efficiency by improving the crystalline of perovskite films.

Abbreviations

DMF: Dimethylformamide; DMSO: Dimethyl sulfoxide; ETL: Electron transport layer; FA: HC(NH₂)₂; FF: Fill factor; FTIR: Fourier-transform infrared spectroscopy; HTL: Hole-transport layer; ITO: Indium tin oxide; J_{sc}: Short-circuit current density; J-V: Current density-voltage; MA: CH₃NH₂; NH₄SCN: Ammonium thiocyanate; OIMHP: Organic-inorganic hybrid metal halide perovskite; PCE: Power conversion efficiency; PMMA: Poly(methyl methacrylate); PSCs: Perovskite solar cells; SEM: Scanning electron microscope; Spiro-OMeTAD: (2,2',9,9'-tetrakis(4-methoxyphenylamine)-9,9'-spirobifluorene); TS-QLE: Theoretical Shockley-Queisser limit efficiency; V_{oc}: Open-circuit voltage; XRD: X-ray diffraction

Acknowledgements

The authors greatly acknowledge the Sichuan University and Ceshigou Analytical Testing Company for the measurement assistance.

Authors' Contributions

ZL and DL wrote the article and did the experiment together. HC, JL, and HZ performed the FTIR, XRD, and SEM data analysis, respectively. YG, SL, and FW revised the article. ZC supervised the whole project and interpreted the results. All authors read and approved the final manuscript.

Funding

This work was supported by the National Natural Science Foundation of China under Grant Nos. 61874150, 61421002, and 61574029. This work was also partially supported by the University of Kentucky. The manuscript was written through contributions of all authors. All authors have given approval to the final version of the manuscript. The authors declare no competing financial interests.

Availability of Data and Materials

All the data are fully available without restrictions.

Competing Interests

The authors declare that they have no competing interests.

Author details

¹State Key Laboratory of Electronic Thin Films and Integrated Devices, and School of Optoelectronic Science and Engineering, University of Electronic Science and Technology of China (UESTC), Chengdu 610054, Sichuan, China.

²Department of Electrical & Computer Engineering, Center for Nanoscale Science & Engineering, University of Kentucky, Lexington, KY 40506, USA.

Received: 6 June 2019 Accepted: 19 August 2019

Published online: 02 September 2019

References

- NREL: National Center For Photovoltaics Home Page. <https://www.nrel.gov/pv/assets/pdfs/best-research-cell-efficiencies-190416.pdf>. Accessed 16 April 2019.
- Turren-Cruz SH, Hagfeldt A, Saliba M (2018) Methylammonium-free, high-performance and stable perovskite solar cells on a planar architecture. *Science* 362(6413):449–453

3. Wang F, Zhang T, Wang Y et al (2019) Steering the crystallization of perovskites for high-performance solar cells in ambient air. *J Mater Chem A* 7(19):12166–12175
4. Wang P, Wu Y, Cai B et al (2019) Solution-processable perovskite solar cells toward commercialization: progress and challenges. *Adv Funct Mater* DOI: <https://doi.org/10.1002/adfm.201807661>
5. Yang Y, Peng H, Liu C et al (2019) Bi-functional additive engineering for high-performance perovskite solar cells with reduced trap density. *J Mater Chem A* 7(11):6450–6458
6. Chen Y, Yang Z, Jia X et al (2019) Thermally stable methylammonium-free inverted perovskite solar cells with Zn^{2+} doped CuGaO_2 as efficient mesoporous hole-transporting layer. *Nano Energy* 61:148–157
7. Zheng X, Deng Y, Chen B et al (2018) Dual functions of crystallization control and defect passivation enabled by sulfonic zwitterions for stable and efficient perovskite solar cells. *Adv Mater* 30(52):e1803428
8. Liu D, Wang Y, Xu H et al (2019) SnO_2 -based perovskite solar cells: configuration design and performance improvement. *Sol RRL* 3(2):1800292
9. Lin Y, Shen L, Dai J et al (2017) π -Conjugated Lewis Base: Efficient trap-passivation and charge-extraction for hybrid perovskite solar cells. *Adv Mater* 29(7):1604545
10. Liu D, Wang Y, She Z et al (2018) Suppressed decomposition of perovskite film on ZnO via a self-assembly monolayer of methoxysilane. *Sol RRL* 2(12):1800240
11. Dong H, Wu Z, Xi J et al (2018) Pseudohalide-induced recrystallization engineering for $\text{CH}_3\text{NH}_3\text{PbI}_3$ film and its application in highly efficient inverted planar heterojunction perovskite solar cells. *Adv Funct Mater* 28(2):1704836
12. Zhao Y, Tan H, Yuan H et al (2018) Perovskite seeding growth of formamidinium-lead-iodide-based perovskites for efficient and stable solar cells. *Nat Commun* 9(1):1607
13. Azam M, Liu K, Yue S et al (2019) The positive function of incorporation of small molecules into perovskite materials for high-efficient stable solar cells. *Sol RRL* 3(3):1800327
14. Gong X, Guan L, Pan H et al (2018) Highly efficient perovskite solar cells via nickel passivation. *Adv Funct Mater* 28(50):1804286
15. Zhou W, Li D, Xiao Z et al (2019) Zwitterion coordination induced highly orientational order of $\text{CH}_3\text{NH}_3\text{PbI}_3$ perovskite film delivers a high open circuit voltage exceeding 1.2 V. *Adv Funct Mater* 2019:1901026
16. Li S, Zhang P, Chen H et al (2017) Mesoporous PbI_2 assisted growth of large perovskite grains for efficient perovskite solar cells based on ZnO nanorods. *J Power Sources* 342:990–997
17. Wang Y, Wu J, Zhang P et al (2017) Stitching triple cation perovskite by a mixed anti-solvent process for high performance perovskite solar cells. *Nano Energy* 39:616–625
18. Wang Y, Li S, Zhang P et al (2016) Solvent annealing of PbI_2 for high-quality crystallization of perovskite films for solar cells with efficiency exceeding 18%. *Nanoscale* 8(47):19654–19661
19. Conings B, Bretschneider SA, Babayigit A et al (2017) Structure-property relations of methylamine vapor treated hybrid perovskite $\text{CH}_3\text{NH}_3\text{PbI}_3$ films and solar cells. *ACS Appl Mater Interfaces* 9(9):8092–8099
20. Jiang Y, Juarez-Perez EJ, Ge Q et al (2016) Post-annealing of MAPbI_3 perovskite films with methylamine for efficient perovskite solar cells. *Mater Horiz* 3(6):548–555
21. Bi D, Yi C, Luo J et al (2016) Polymer-templated nucleation and crystal growth of perovskite films for solar cells with efficiency greater than 21%. *Nat Energy* 1:16142
22. Zhang M, Dai S, Chandrabose S et al (2018) High-performance fused ring electron acceptor-perovskite hybrid. *J Am Chem Soc* 140(44):14938–14944
23. Zhang Z, Zhou Y, Cai Y et al (2018) Efficient and stable $\text{CH}_3\text{NH}_3\text{PbI}_{3-x}(\text{SCN})_x$ planar perovskite solar cells fabricated in ambient air with low-temperature process. *J Power Sources* 377:52–58
24. Yang G, Wang C, Lei H et al (2017) Interface engineering in planar perovskite solar cells: energy level alignment, perovskite morphology control and high performance achievement. *J Mater Chem A* 5(4):1658–1666
25. Watthage SC, Song Z, Shrestha N et al (2017) Enhanced grain size, photoluminescence, and photoconversion efficiency with cadmium addition during the two-step growth of $\text{CH}_3\text{NH}_3\text{PbI}_3$. *ACS Appl Mater Interfaces* 9(3):2334–2341
26. Zhang H, Hou M, Xia Y et al (2018) Synergistic effect of anions and cations in additives for highly efficient and stable perovskite solar cells. *J Mater Chem A* 6(19):9264–9270
27. Yang S, Liu W, Zuo L et al (2016) Thiocyanate assisted performance enhancement of formamidinium based planar perovskite solar cells through a single one-step solution process. *J Mater Chem A* 4(24):9430–9436
28. Zhang X, Wu G, Yang S et al (2017) Vertically oriented 2D layered perovskite solar cells with enhanced efficiency and good stability. *Small* 13(33):1700611
29. Zhang X, Wu G, Fu W et al (2018) Orientation regulation of phenylethylammonium cation based 2D perovskite solar cell with efficiency higher than 11%. *Adv Energy Mater* 8(14):1702498
30. Wang F, Jiang X, Chen H et al (2018) 2D-quasi-2D-3D hierarchy structure for tin perovskite solar cells with enhanced efficiency and stability. *Joule* 2(12):2732–2743
31. Jiang Q, Zhang L, Wang H et al (2016) Enhanced electron extraction using SnO_2 for high-efficiency planar-structure $\text{HC}(\text{NH}_2)_2\text{PbI}_3$ -based perovskite solar cells. *Nat Energy* 1:16177
32. Liu D, Li S, Zhang P et al (2017) Efficient planar heterojunction perovskite solar cells with Li-doped compact TiO_2 layer. *Nano Energy* 31:462–468
33. Heo JH, You MS, Chang MH et al (2015) Hysteresis-less mesoscopic $\text{CH}_3\text{NH}_3\text{PbI}_3$ perovskite hybrid solar cells by introduction of Li-treated TiO_2 electrode. *Nano Energy* 15:530–539
34. Zhang P, Wu J, Wang Y et al (2017) Enhanced efficiency and environmental stability of planar perovskite solar cells by suppressing photocatalytic decomposition. *J Mater Chem A* 5(33):17368–17378
35. Chen Y, Yang Z, Wang S et al (2018) Design of an inorganic mesoporous hole-transporting layer for highly efficient and stable inverted perovskite solar cells. *Adv Mater* 30(52):e1805660

Publisher's Note

Springer Nature remains neutral with regard to jurisdictional claims in published maps and institutional affiliations.

Submit your manuscript to a SpringerOpen[®] journal and benefit from:

- Convenient online submission
- Rigorous peer review
- Open access: articles freely available online
- High visibility within the field
- Retaining the copyright to your article

Submit your next manuscript at ► [springeropen.com](https://www.springeropen.com)